Significantly enhanced temperature-dependent selectivity for NO_2 and H_2S detection based on In_2O_3 nano-cubes prepared by CTAB assisted solvothermal process

Zhijie Li[1*], Shengnan Yan[1], Sun Mengxuan[1], Hao Li[1], Zhonglin Wu[1], Sun Mengxuan[1], Wenzhong Shen[2], Yong Qing Fu[3*]

[1]School of Physics, University of Electronic Science and Technology of China, Chengdu, 610054, P. R. China

[2]State Key Laboratory of Coal Conversion, Institute of Coal Chemistry, Chinese Academy of Science, Taiyuan, 030001, China

[3]Faculty of Engineering and Environment, Northumbria University, Newcastle Upon Tyne, NE1 8ST, UK

Abstract

It is a huge challenge to develop a highly precision sensor with good selectivities for two different types of toxic gases. In this work, In_2O_3 nano-cubes, prepared using a cetyltrimethyl ammonium bromide assisted solvothermal process, were used to make gas sensors for H_2S and NO_2 detections. The In_2O_3 nano-cube based sensor exhibited a good temperature-dependent selectivity toward H_2S and NO_2. At room temperature of 25 □, the sensor exhibited a good selectivity towards H_2S with a high response (1461 for 60 ppm H_2S), fast response/recovery times (82 s/102 s) and a superior detection limit (0.005 ppm). Whereas at an operation temperature of 100 □, the sensor showed a poor sensitivity to H_2S, but an excellent selectivity towards NO_2 with a high response (336 for 100 ppm NO_2), fast response/recovery times (18 s/31 s) and a superior detection limit (0.001 ppm). The sensor also showed good reversibility, reproducibility and long-term stability at two optimized operation temperatures. The different sensing mechanisms for H_2S and NO_2 were discussed and the temperature dependent selectivity was explained.

Keywords: In_2O_3, nano-cube, NO_2, H_2S, gas sensor

1 Introduction

Hydrogen sulfide (H_2S) and nitrogen dioxide (NO_2) are two dangerous gases, which are daily released from vehicles and industrial processes. Because of their serious hazards to health and environment, the safe concentration limits of H_2S and NO_2 in the ambient established by American National Institute for Occupational Safety and Health (NIOSH) are 10 ppm and 1 ppm, respectively. Therefore, there are significant interests to develop gas sensors to detect for these two gases [1, 2]. The resistance type gas sensors based on metal oxides are the mostly studied ones, and the commonly reported oxides include ZnO [3, 4], In_2O_3 [5-7], WO_3 [8, 9], TiO_2[10], Fe_2O_3[11-13], SnO_2[14], CuO[15] and CeO_2[16]. Although there are many reports of either NO_2 sensors or H_2S sensors in recent years, so far there are few studies about the development of dual-function gas sensors which can efficiently detect both NO_2 and H_2S at different temperatures.

Among these metal oxides, nano-sized In_2O_3 is considered as one of the promising candidate materials to detect many hazardous gases including H_2S [17], NO_2[18], CO[19], H_2[20] and C_2H_5OH[21] etc. In particular, NO_2 or H_2S sensors based on In_2O_3 nanostructures have been frequently reported in recent years [6, 22-25]. It is well known that morphology and microstructure of these metal oxides prominently influence their sensing properties. Therefore, there are many studies to synthesize various morphologies of In_2O_3 in order to detect NO_2 or H_2S gases, including nanowires [22], nanospheres[23], nanofibers [24], nanorods[7], nanosheets [25], nanoparticles [6, 26, 27], etc. However, most of these studies are focused on sensing one specific gas of

either NO_2 or H_2S. As far as we have searched, there is no any report to apply In_2O_3 based gas sensors for detection of both NO_2 and H_2S gases operated at different temperatures.

The objective of this paper is to synthesize In_2O_3 nano-cube sensing materials using a cetyltrimethyl ammonium bromide (CTAB) assisted solvothermal process, and then apply these nano-cubes for fabricating gas sensors to detect NO_2 and H_2S. These gas sensors exhibited good temperature-dependent selectivity and excellent sensing performance toward both H_2S and NO_2.

2 Experimental

2.1 Preparation and characterization of In_2O_3 nano-cubes

In_2O_3 nano-cubes were prepared using the CTAB assisted solvothermal and subsequent calcination processes. Firstly, $InCl_3 \cdot 4H_2O$ of 0.440 g was dissolved into 20 ml ethanol, and NaOH of 0.6 g were dissolved into 20 ml deionized water, respectively. The above $InCl_3 \cdot 4H_2O$ ethanol solution (0.075 mol/L) and NaOH aqueous solution (0.75 mol/L) were mixed under a vigorous stirring process. CTAB of 0.273 g was added into the above mixed solution and stirred for one hour under a magnetic stirring to form a sol, which was then transferred into a Teflon-lined autoclave and placed in an oven for the solvothermal reactions at 180 □ for 12 hrs. Finally, the solvothermal product was filtered, washed and dried at 60 □ for 6 hrs to obtain $In(OH)_3$ powders. In_2O_3 nano-cubes were finally obtained by calcining the $In(OH)_3$ powder at 500 □ in air for 2 hrs.

2.2 Sample Characterization

Selected area electron diffraction (SAED) patterns and transmission electron

microscopy (TEM) images were obtained using a JEOL JEM-2100F TEM instrument with an accelerating voltage of 200 kV. Scanning electron microscope (SEM) image of the sample was obtained using an Inspect F50 SEM instrument. X-ray diffraction (XRD) patterns were obtained using a Rigaku MiniFlex II X-ray diffractometer (with a Cu Ka radiation source, 40 kV and 15 mA). An X-ray photoelectron spectroscope (XPS, Kratos Axis-Ultra DLD apparatus) with Mg Ka radiation was used to obtain the chemical binding of different elements in the oxides. Surface area of the sample was measured based on the Brunauer-Emmett-Teller (BET) method using a Micromeritics ASAP 2020 Analyzer, measured at a temperature of −196 □. The band gap value was measured using a diffuse reflectance spectra (DRS, UV-2101 Shimadzu), and $BaSO_4$ was used as the reference.

2.3 Gas sensor fabrication and measurement

Aluminum oxide ceramic tube (with a length of 4 mm and a diameter of 1 mm) with two gold electrodes on its surface was used to fabricate the gas sensor. To coat an In_2O_3 layer on the ceramic tube, 40 mg of In_2O_3 powder was dissolved in 10 ml alcohol and ultrasonically agitated for 20 min to obtain a homogeneous suspension. The In_2O_3 suspension was then dip-coated onto surface of aluminum oxide ceramic tubes until a continuous In_2O_3 film was formed. Finally, the coated sample was dried at 120 □ for 2 hrs. The thickness of the In_2O_3 layer was about 100 μm.

A Ni–Cr alloy resistive heater was placed inside the ceramic tube to control the operating temperature of the sensor. The sensor was placed inside a glass testing container of 2 liters in volume. The diluted NO_2 or H_2S gas was injected into the

container using a precision micro-injector. A Keithley 2400 SourceMeter was connected to the gold electrodes of the sensor to measure the changes of electric resistance of the sensor. The applied voltage used in the gas sensing testing system was 1 V. The response (R) of the sensor is defined as R_{air}/R_{H2S} for the reducing gas of H_2S, and it is defined as R_{NO2}/R_{air} for the oxidizing gas of NO_2, where R_{air} is the electrical resistance of the sensor measured in air, R_{H2S} and R_{NO2} are the electrical resistance data measured in the diluted gases of H_2S or NO_2, respectively. After the sensor's response was reached its largest equilibrium value, the sensor was continuously exposed to the target gas for another ~100 s in order to obtain a stable response value. The response time is defined as the time for the increase of the sensor's response to reach 90% of its largest equilibrium value after the target gas is injected, and the recovery time is defined as the time for the decrease to 10% of the largest equilibrium value after the target gas is removed from the chamber.

3 Results and discussion

3.1 Microstructural analysis

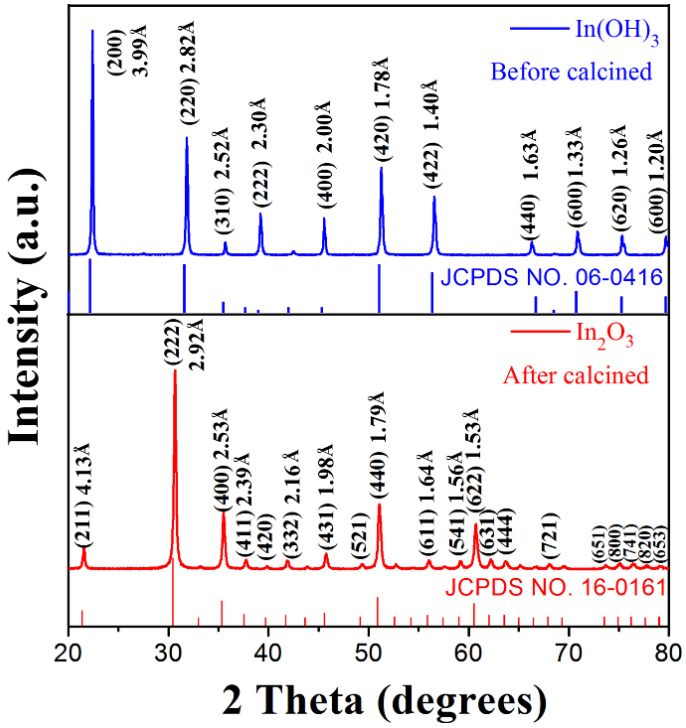

Fig. 1 XRD patterns of samples before and after calcination at 500 □ in air.

XRD patterns of samples before and after calcination at 500 □ are shown in Fig. 1. All the diffraction peaks of the samples before the calcination are corresponding to $In(OH)_3$ crystal structure (JCPDS Card No. 16-0161). After calcined at 500 □, the $In(OH)_3$ was transformed into cubic In_2O_3 crystal (JCPDS Card No. 06-0416). No other characteristic peaks of impurities were detected, indicating that the pure In_2O_3 was obtained after calcination at 500 □. According to Scherrer equation, the estimated average crystal size of the In_2O_3 is ~48.4 nm.

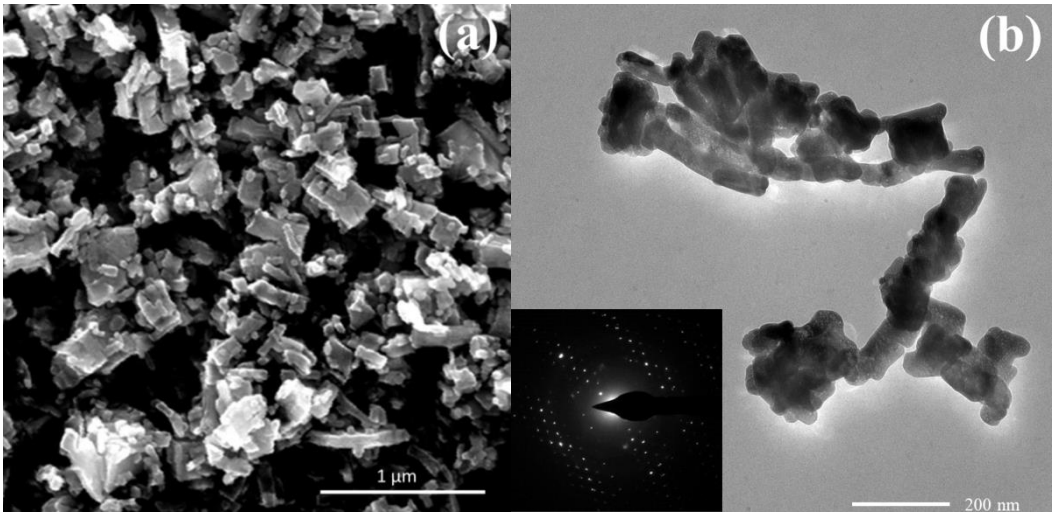

Fig. 2 (a) SEM and (b) TEM images of the In_2O_3 nano-cubes (the inset in b is its corresponding SAED pattern).

SEM and TEM images of In_2O_3 are shown in Fig. 2, and another low-magnification TEM image is presented in the Fig. S1 in the Supporting Information. It can be seen that the In_2O_3 sample is mainly composed of many nano-cubes, although there are also tiny amount of nano-rods. The average diameter of In_2O_3 nano-cubes was estimated to be ~50 nm, which is consistent with the calculated average size from XRD analysis. The SAED pattern (see the inset in Fig. 2b) can be indexed to cubic phase of In_2O_3, indicating its highly crystalline structure. Based on the BET analysis from the nitrogen adsorption isotherm, the obtained BET surface area of the In_2O_3 nano-cubes is 11.96 $m^2 \cdot g^{-1}$. In_2O_3 is a wide band-gap semiconductor material, and its optical bandgap changes with its size and shape, especially when it is in a nanoscale structure. The DRS result of the In_2O_3 nano-cubes is shown in Fig. 3. The obtained optical band-gap (Eg) is ~3.37 eV, which is similar to the value reported in literature [28].

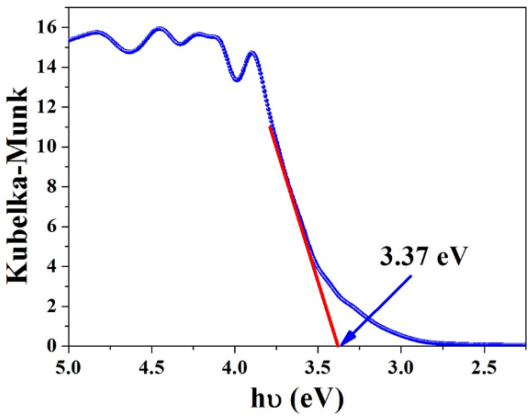

Fig. 3. The diffuse reflectance spectrum of the In_2O_3 nano-cubes.

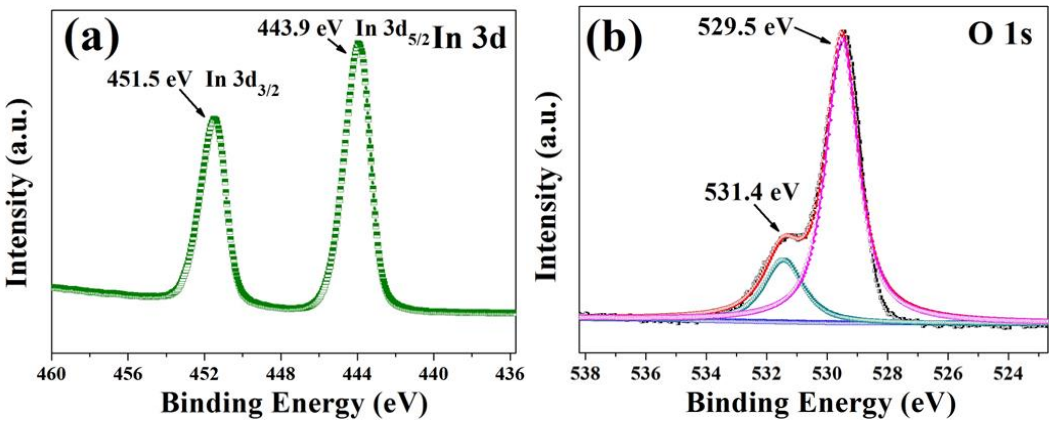

Fig. 4. XPS spectra of the In_2O_3 nano-cubes: (a) In 3d and (b) O 1s.

XPS spectra of the In_2O_3 nano-cubes are shown in Fig. 4. In the XPS spectrum of In 3d (see in Fig. 4a), the binding energy peaks at 443.9 and 451.5 eV are attributed to In $3d_{5/2}$ and In $3d_{3/2}$ of In^{3+} ions, respectively, which proves the formation of In_2O_3 [22]. Two peaks are observed in the O 1s spectrum, in which the peak at 529.5 eV is corresponding to the O^{2-} ions in the crystal lattice of the In_2O_3, and the peak at 531.4 eV is corresponding to the chemisorbed oxygen ions on the surface of In_2O_3 [27]. Based on the calculation result of XPS integral area, the surface atomic ratio of the In and O is 37:63, which means that there is a high concentration of oxygen ions on the surface of In_2O_3 nano-cubes. Furthermore, the atomic content of chemisorbed oxygen ions was as high as 20.8% in the total oxygen atoms, indicating that there are plenty of

chemisorbed oxygen ions on the surface.

3.2 Gas sensing properties

3.2.1 NO_2 gas sensing properties

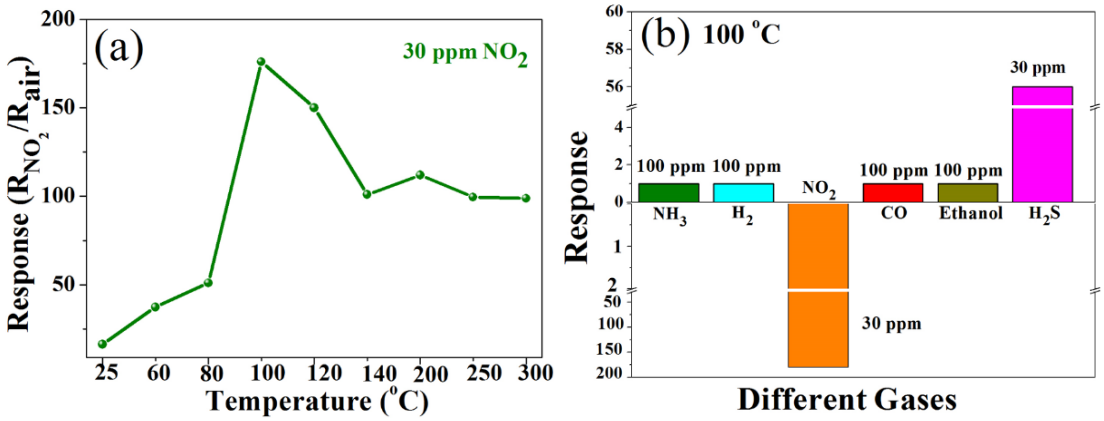

Fig. 5. (a) Response values of the In_2O_3 nano-cubes based gas sensor to 30 ppm of NO_2 at different operating temperatures, and (b) response values to different gases operated at the operating temperature of 100 ℃.

The I-V curves of the gas sensor based on In_2O_3 nano-cubes measured at 25 □ and 100 □ (see the Fig. S2 in the Supporting Information) show a linear behavior. This is a typical phenomenon of Ohmic contact behavior. It was previously reported that the contact of the In_2O_3 with the Au electrodes normally has a Schottky contact behavior [29, 30]. However, in this study, the electrical resistance generated between the In_2O_3 nano-cubes (normally with the Ohmic contact behavior) is much larger than that between the In_2O_3 and Au electrode. Therefore, the I-V curves of this In_2O_3 gas sensor exhibit an Ohmic behavior, rather than a typical Schottky contact behavior [16]. When the temperature is increased from 25 □ to 100 □, the resistance of gas sensor is decreased from 782 KΩ to 175 KΩ..

The responses of the gas sensor to 30 ppm NO_2 gas at different temperatures from 25

□ to 300 □ were measured. According to the response/recovery curves (see the Fig. S3 in Supporting Information), the response values were calculated and the results are shown in Fig. 5a. The sensor exhibits a good response to NO_2 at different temperatures, and the maximum response value of 176 is obtained at 100 □. Therefore, the optimum operation temperature for the NO_2 gas of this gas sensor should be 100 □. Generally it is preferred that the detection of NO_2 should be operated at a lower temperature, better at room temperature [31]. Therefore, in the following studies, the sensing tests using the In_2O_3 nano-cubes based gas sensor were performed at both 25 □ and 100 □.

To investigate the NO_2 selectivity of the In_2O_3 nano-cubes based gas sensor, its responses to different gases (including NH_3, H_2, CO, ethanol, H_2S and NO_2) were tested at the operating temperature of 100 □. From the results shown in Fig. 5b, the gas sensor shows a high response value to 30 ppm of NO_2. However, it shows little response values to other tested gases of NH_3, H_2, CO and ethanol with a concentration of 100 ppm. For the 30 ppm of H_2S gas, the response value is 56, which is much less than that for NO_2. Therefore, the gas sensor shows a good NO_2 gas selectivity at the operating temperature of 100 □.

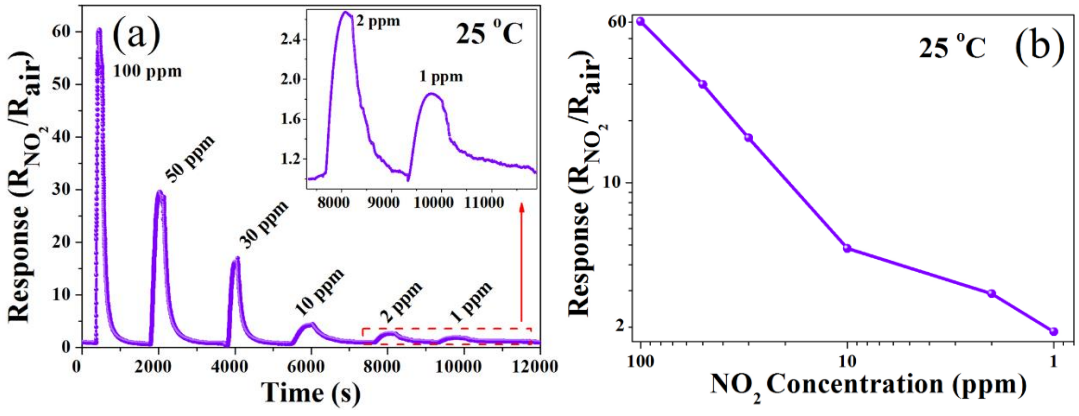

Fig. 6. (a) Response/recovery curves and (b) response value of the In_2O_3 nano-

cubes based gas sensor to different concentrations of NO_2 from 100 ppm to 1 ppm at room temperature.

Fig. 6a shows the response/recovery curves of the In_2O_3 nano-cubes based gas sensor exposed to different concentrations of NO_2 from 100 ppm to 1 ppm at room temperature. This gas sensor shows a good reversibility at room temperature. Its response values are dependent on the NO_2 concentration (as shown in Fig 6b). For 100 ppm of NO_2, the response value is 60.4, and the response and recovery times are 49 s and 197 s, respectively. The detection limit of this sensor is 1 ppm when operated at room temperature.

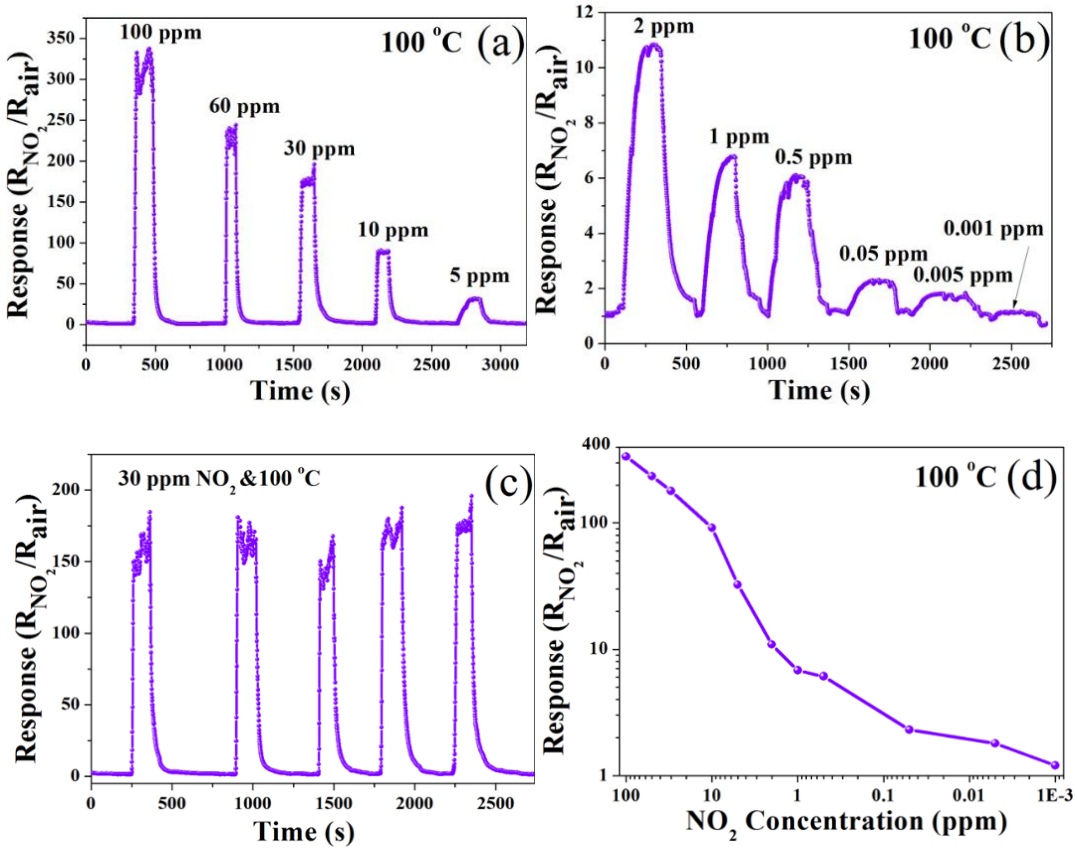

Figs. 7 (a) and (b) Response/recovery curves of the In_2O_3 nano-cubes based gas sensor to NO_2 with different concentrations from 100 ppm to 0.001 ppm at 100 □, (c) the repeated response/recovery curves to 30 ppm of NO_2 by successively testing at

100 □, (d) the response value to different concentrations of NO_2 at 100 □.

Figs. 7 shows the NO_2 sensing peformance of the In_2O_3 sensor measured at 100 □. The gas sensor shows a good reversibility for the NO_2 detection. When the measurement temperatures are increased from 25 □ to 100 □, the response values are increased and the response/recovery times of the sensor are decreased remarkably. For examples, when exposed to 100 ppm NO_2 at 100 □, the response value of the sensor is increased to 336, and the response and recovery times are decreased to 18 s and 31 s, respectively. It is also worthy to mention that even for 0.001 ppm of NO_2, the sensor still shows an obvious response of 1.2. Therefore, this In_2O_3 sensor show a high sensitivity, fast response/recovery, and a low detection limit for the NO_2 at the working temperature of 100 □. After the sensor is successively tested in 30 ppm of NO_2 for four times, the response/recovery curves (shown in Fig. 7c) exhibit good reproducibility.

Table 1 Comparisons of NO_2 sensing properties of In_2O_3 gas sensor in this work with those reported in literature.

Material Structures	Working Temp.	Conc. (ppm)	Response	Response /recovery time	Detection limit(ppm)	Ref.
Pd-In_2O_3 nanowire	300 □	3	3.4	60 s/365 s	3	[22]
In_2O_3 nanosphere	120 □	0.5	217.5	148 s/72 s	0.01	[23]
In_2O_3 Nanoparticle	300 □	1.2	1.09	120 s/39 s	0.5	[26]
Pd-In_2O_3	135 □	50	4080	120 s/90 s	0.5	[32]
Ni-doped In_2O_3	58 □	0.5	178	9 min/~10 min	0.01	[33]
In_2O_3 nanorod bundle	100 □	1	87	177 s/152 s	0.04	[34]
In_2O_3–graphene	25 □	30	8.25	4 min/24 min	5	[35]
In_2O_3 microcube	60 □	30	1884	~300 s/~200 s	0.5	[5]
In_2O_3 microsphere	250 □	20	37	5 s/20 s	5	[36]

In_2O_3 nanosheets	250 □	50	164	5 s/14 s	1	[25]
graphene oxide-In_2O_3	150 □	0.5	22.3	170 s/280 s	-	[18]
In_2O_3 Cubes-Graphene	25 □	5	37.81%[a]	3 min/no recovery	1	[37]
In_2O_3 thin film	180 □	1	5	160 s/260 s	1	[38]
In_2O_3 °Œtahedron	130 □	50	120	200 s/300 s	0.05	[39]
In_2O_3 nano-cubes	25 □	100	60.4	49 s/197s	1	This work
In_2O_3 nano-cubes	100 □	100	336	18 s/31 s	0.001	This work

[a] Response = $(R_a - R_g)/R_a \times 100\%$.

Table 1 summarizes the reported NO_2 sensing properties of various In_2O_3 based gas sensors from literature. Compared with most of these reported sensors, the In_2O_3 nano-cube based gas sensor developed in this study shows a lower working temperature, higher response values and the lowest detection limit. Furthermore, the response/recovery times are also much shorter than most of other In_2O_3 based NO_2 gas sensors reported in literature.

3.2.2 H_2S gas sensing properties

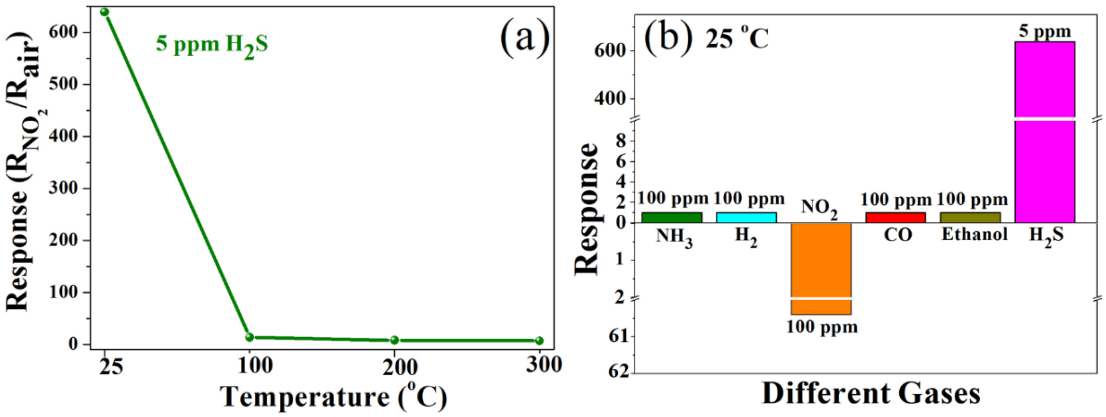

Fig. 8 (a) Response values of In_2O_3 nano-cubes based gas sensor to 5 ppm of H_2S at different operating temperatures, and (b) response values to different gases operated at room temperature of 25 □.

To obtain the optimum operation temperature to H_2S, we have measured the response/recovery curves of the In_2O_3 sensor to 5 ppm H_2S from 25 □ to 300 □ (see

the Fig. S4 in Supporting Information). The response values are shown in Fig. 8a. The sensor exhibits a significantly high response to H_2S when measured at room temperature, whereas the response value is gradually decreased with the increase in the operating temperature above 25 □. Therefore, the optimum operation temperature for the H_2S gas is 25 □.

At room temperature, the responses of the In_2O_3 based sensor to different gases (including NH_3, H_2, CO, NO_2, ethanol and H_2S) were tested. From the results shown in Fig. 8b, the sensor shows a high response of 639 to 5 ppm of H_2S. Whereas it shows little responses to other tested gases. Therefore, the In_2O_3 nano-cube based gas sensor has a good H_2S selectivity at room temperature.

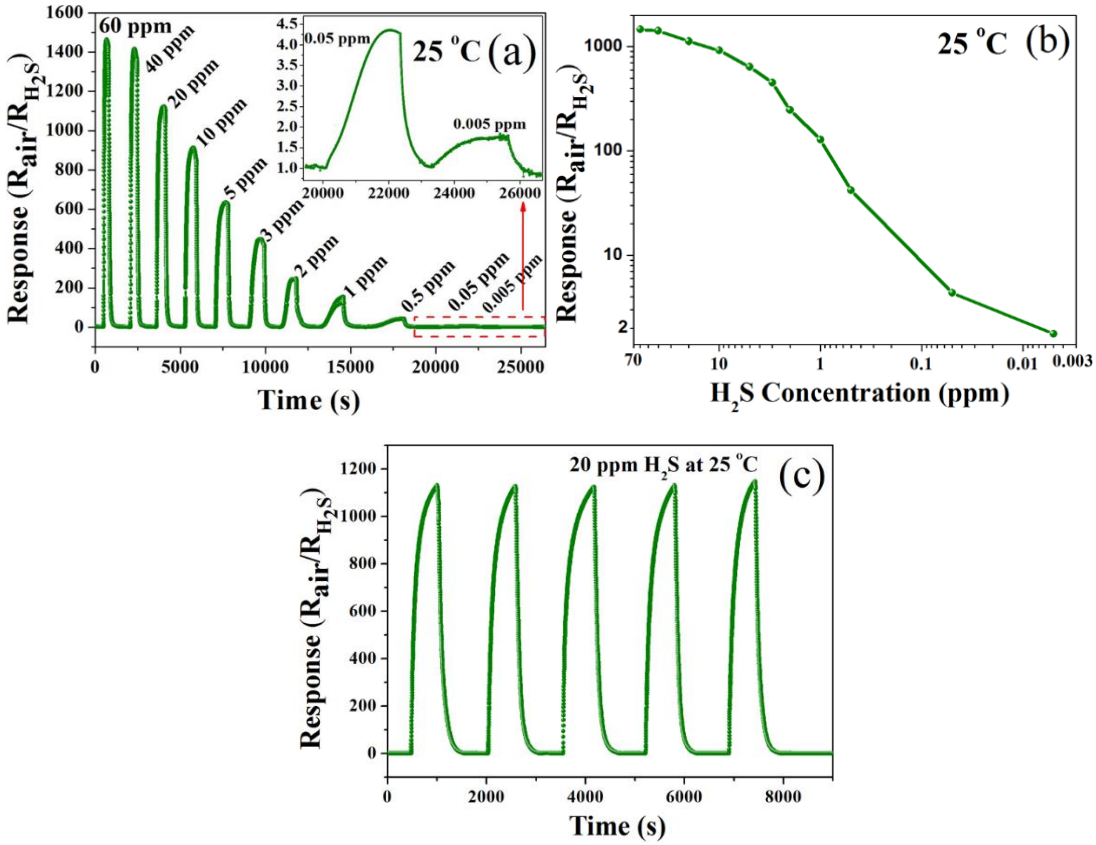

Fig. 9. (a) Response/recovery curves and (b) response values of the In_2O_3 nano-cubes based gas sensor to H_2S gas with different concentrations from 60 ppm to 0.005

ppm at room temperature, (c) repeated response/recovery curves of five time exposure to 20 ppm of H_2S gas by successively testing the sensor.

Fig. 9a shows the response/recovery curves of the In_2O_3 based gas sensor to different concentrations of H_2S at room temperature. The sensor shows a steady baseline in air before and after the sensing tests, meaning that the sensor has good reversibility for the H_2S detection. Fig. 9b shows the response/recovery curves of the sensor exposed to 20 ppm H_2S after successively tested for five times. The gas sensor exhibits almost same response/recovery curves with the same response value of 1126 in all five repeated tests, indicating that the gas sensor has a good reproducibility. The response values of the sensor are shown in Fig. 9c. It can be seen that the response values are increased with the increase of the concentration of H_2S. The response value to 60 ppm H_2S is as large as 1461 with the response/recovery times of 82 s/102 s. In addition, the gas sensor still has an obvious response value of 1.8 when the concentration of H_2S is as low as 0.005 ppm. Therefore, the In_2O_3 nano-cube based gas sensor has not only a high response, but also a superior detection limit to H_2S.

Table 2 compares the H_2S sensing properties of In_2O_3 gas sensor in this work with those reported in the literature. Compared with most of the reported gas sensors, the gas sensor developed in this study shows the highest response value, except for the Mg-In_2O_3 nanotubes based sensor reported in Ref [40]. Although the Mg-In_2O_3 sensor shows a higher response value, a full recovery of its signals is difficult to achieve [38]. Furthermore, the In_2O_3 sensor in this study has the lowest detection limit as listed in Table 2.

Table 2 Comparisons of H_2S sensing properties of In_2O_3 based gas sensor in this work with those reported in literature.

Material Structures	Working Temp.	Conc. (ppm)	Response	Response/recovery time	Detection limit (ppm)	Ref.
In_2O_3 porous film	300 □	50	30	16 s/30 s	1	[17]
CuO-In_2O_3 nanofiber	150 □	5	9170%[a]	~200 s/no recovery	0.4	[24]
V-In_2O_3 nanofiber	90 □	50	13.9	15 s/18 s	1	[41]
Eu-In_2O_3 nanobelt	260 □	100	5.74	11 s/13 s	5	[42]
Mg-In_2O_3 nanotube	130 □	10	1959.77	~75 s/ no recovery	-	[40]
In_2O_3/WO_3 composite	150 □	10	143	5.5 min/16 min	0.5	[43]
In_2O_3 whisker	25 □	10	30	4 min/2 h	0.2	[44]
In_2O_3 nanoparticle	25 □	2	200%[a]	30 min/5 min	0.02	[27]
PVA-In_2O_3 film	25 □	1	1.9	~5 min/31 min	0.5	[45]
In_2O_3/CuO nanofiber	25 □	100	2.23	5.3 s/--	1	[46]
In_2O_3 nanotube	25 □	50	320.14	45 s/127 s	1	[47]
In_2O_3 nano-cubes	25 □	60	1461	82 s/102s	0.005	This work

[a] Response = $(R_a - R_g)/R_a \times 100\%$.

3.2.3 Stability of the In_2O_3 nano-cubes based gas sensor

In order to investigate the long-term stability of the In_2O_3 sensor, its responses to both H_2S and NO_2 were repeatedly tested in a month at their different optimum operation temperatures, and the results are shown in Fig. 10. The fluctuations of the response value to 20 ppm of H_2S and 30 ppm of NO_2 are lower than 3%, indicating that the In_2O_3 based gas sensor have a good stability for detection of both NO_2 and H_2S gases.

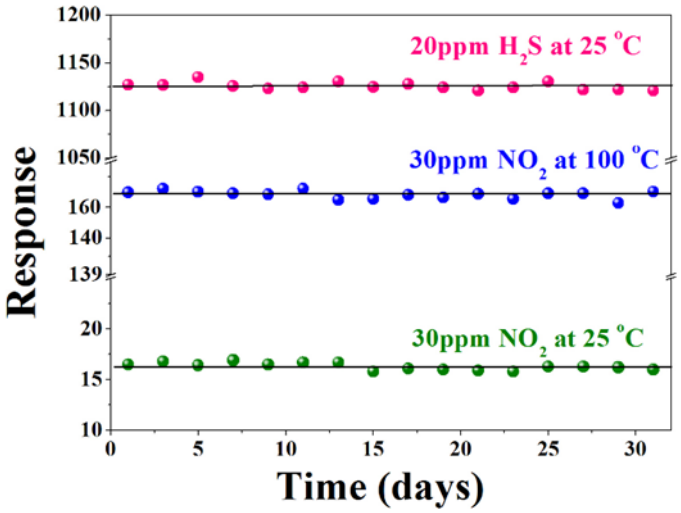

Fig. 10 Stability of the In_2O_3 nano-cube based gas sensor with repeated tests of H_2S and NO_2 in a month.

3.3 Gas sensing mechanisms

For the n-type semiconductor materials such as In_2O_3, the mechanism for NO_2 and H_2S gas sensing are all related to the surface controlled reaction mechanisms as reported in References [27, 39]. In air, oxygen molecules are absorbed on the surfaces of In_2O_3 nano-cubes, and they capture free electrons from the In_2O_3 to form chemisorbed oxygen ions (such as O^{2-}, O^- and O_2^-) [48] . This process will result in formation of an electron-depletion layer on the surface of In_2O_3 nano-cube, and thus increase the gas sensor's resistance. These types of chemisorbed oxygen ions are dependent on the operation temperature of the gas sensor. When the temperature is lower than 100 □, the chemisorbed oxygen ions are O_2^-, whereas they are mainly O^- at an operation temperature from 100 □ to 300 □ [48].

Effect of temperature on the sensing property is strongly related to the surface processes of adsorption, reaction and desorption. At the operation temperature below 100 □, after the In_2O_3 sensor is exposed in NO_2, the NO_2 molecules can be easy

absorbed on the surface of In_2O_3, and then result in the following reactions [49-51]:

$$NO_{2(g)} + e^- \rightarrow NO_{2(ads)}^- \quad (1)$$

$$NO_{2(g)} + O_2^-{}_{(ads)} + 2e^- \rightarrow NO_2^-{}_{(ads)} + 2O^- \quad (2)$$

However, the above reactions are not easily triggered (less energy favorite) and the desorption of NO_2^- is also slow in the recovery process. This should be reason why the response/recovery times are quite long as shown in Fig. S3. Also the response is very low at low temperatures.

When the temperature is increased to 100 □, the absorbed NO_2 molecules will react with the chemisorbed O^- according to the following reaction equation [51]:

$$NO_2^-{}_{(ads)} + O^-{}_{(ads)} + 2e^- \leftrightarrow NO_{(g)} + 2O^{2-}{}_{(ads)} \quad (3)$$

At such a temperature, thermal energy of the NO_2 molecules is high enough, and can overcome the activation energy barrier of the reaction. More NO_2 molecules can react with the chemisorbed O^- species. Because the above reaction will trap free electrons from the conduction band of In_2O_3 nano-cubes, the electron concentration on the surface of the In_2O_3 nano-cubes will be reduced. The thickness of electron-depletion layer region is decreased, and consequently the resistance of the sensor is increased. Therefore, the sensor's sensitivity is increased.

However, when the operation temperature is increased further above 100 □, the absorbed NO_2 molecules will be significantly reduced. Their reactions with the surface chemical-absorbed oxygen species will be reduced, thus decreasing the sensitivity of the gas sensor.

When the gas sensor is exposed to be H_2S gas at room temperature, the chemisorbed

O_2^- ions on the surfaces of In_2O_3 will react with the H_2S molecules as described using the following reaction [52]:

$$H_2S_{(g)} + 3/2O_2^-{}_{(ads)} \leftrightarrow H_2O_{(g)} + SO_{2(g)} + 3/2e^- \quad (4)$$

Consequently, electrons will be released to the electron-deletion region on the In_2O_3 surface, which will reduce the electrical resistance of the sensor. In addition, the sulfuration process of In_2O_3 at room temperature is also responsible for the decrease of the sensor's electrical resistance [53]. The H_2S molecules can react with In_2O_3 to form In_2S_3 on the surface of In_2O_3 nano-cubes according to the following equations [54]:

$$In_2O_{3(s)} + 3H_2S_{(g)} \rightarrow In_2S_{3(s)} + 3H_2O_{(g)} \quad (\Delta G = -1318.6 \text{ kJ mol}^{-1}) \quad (5)$$

$$In_2S_{3(s)} + 9/2O_{(g)} \rightarrow In_2O_{3(s)} + 3SO_{2(g)} \quad (\Delta G = -1318.6 \text{ kJ mol}^{-1}) \quad (6)$$

The Gibbs free energy changes (ΔG) of the chemical reactions (5) and (6) are –161.7 and –1318.6 kJ mol^{-1} at 25 □, respectively. This means that these two chemical reactions are spontaneously occurring with the consideration of thermodynamics. The sulfuration of In_2O_3 in H_2S gas (e.g. formation of In_2S_3) and the desulfuration of In_2S_3 in air can happen at room temperature. This has been proved by Xu et al using Raman spectrum [54]. Because the formed In_2S_3 has a higher conductivity than In_2O_3, the electrical resistance will be remarkably increased, thus resulting in a significant response.

With the increase of temperature above room temperature, the ΔG value of chemical reaction (5) will be increased. This indicates that the sulfuration reaction will be restricted, and less In_2S_3 will be formed on the surface of In_2O_3. As a result, the sensitivity to the H_2S will be significantly decreased.

Clearly, the reaction of the oxidizing gas of NO_2 with the chemisorbed oxygen ions on the sensor's surface will release electrons into In_2O_3. On the contrary, the reaction of reducing gas of H_2S with the chemisorbed oxygen ions will extract electrons from the In_2O_3. Therefore, the electrical resistance of the In_2O_3 based gas sensor will be increased when exposed to NO_2, but it will be decreased when exposed to H_2S. Therefore, the gas sensor exhibits totally opposite changes in resistance values when exposed to NO_2 and H_2S, respectively, which allows the sensor to easily distinguish these two gases.

4 Conclusions

In summary, the In_2O_3 nano-cubes were synthesized using the CTAB assisted solvothermal mothed, and then used to fabricate a dual-function NO_2 and H_2S gas sensor. At room temperature of 25 □, the gas sensor exhibited a good selectivity towards H_2S gas. When the operating temperature was increased to 100 □, the sensitivity to H_2S was decreased dramatically, but it showed an excellent selectivity towards NO_2 gas at this temperature. This gas sensor has high response, fast response/recovery time, good reversibility and repeatability, and superior low detection limits in detection of both of NO_2 and H_2S gases. Therefore, the In_2O_3 nano-cubes based gas sensor should be very promising in detection of both the NO_2 and H_2S gases at low operating temperature.

Acknowledgements

Funding supports from UK Engineering Physics and Science Research Council

(EPSRC EP/P018998/1), Newton Mobility Grant (IE161019) through Royal Society and NFSC, and Royal academy of Engineering UK-Research Exchange with China and India are also acknowledged.

References

[1] R. Kumar, N. Goel, M. Kumar, High performance NO_2 sensor using MoS_2 nanowires network, Appl. Phys. Lett. 112 (2018) 053502.

[2] T. Xu, Y. Pei, Y. Liu, D. Wu, Z. Shi, J. Xu, Y. Tian, X. Li, High-response NO_2 resistive gas sensor based on bilayer MoS_2 grown by a new two-step chemical vapor deposition method, J. Alloy. Compd., 725 (2017) 253-259.

[3] R. Kumar, O. Al-Dossary, G. Kumar, A. Umar, Zinc Oxide Nanostructures for NO_2 Gas-Sensor Applications: A Review, Nano-Micro lett. 7 (2015) 97-120.

[4] S.D. Shinde, G.E. Patil, D.D. Kajale, V.B. Gaikwad, G.H. Jain, Synthesis of ZnO nanorods by spray pyrolysis for H_2S gas sensor, J. Alloy. Compd., 528 (2012) 109-114.

[5] S.T. Navale, C. Liu, Z. Yang, V.B. Patil, P. Cao, B. Du, R.S. Mane, F.J. Stadler, Low-temperature wet chemical synthesis strategy of In_2O_3 for selective detection of NO_2 down to ppb levels, J. Alloy. Compd. 735 (2018) 2102-2110.

[6] S.C. Zhang, Y.W. Huang, Z. Kuang, S.Y. Wang, W.L. Song, D.Y. Ao, W. Liu, Z.J. Li, Solvothermal Synthesized In_2O_3 Nanoparticles for ppb Level H_2S Detection, Nanosci. Nanotech. Let. 7 (2015) 455-461.

[7] S. Yan, Z. Li, H. Li, Z. Wu, J. Wang, W. Shen, Y.Q. Fu, Ultra-sensitive room-temperature H_2S sensor using Ag–In_2O_3 nanorod composites, J. Mater. Sci. (2018).

[8] S. Poongodi, P.S. Kumar, D. Mangalaraj, N. Ponpandian, P. Meena, Y. Masuda, C. Lee, Electrodeposition of WO_3 nanostructured thin films for electrochromic and H_2S gas sensor applications, J. Alloy. Compd., 719 (2017) 71-81.

[9] P. Zhou, Y. Shen, S. Zhao, G. Li, Y. Yin, R. Lu, S. Gao, C. Han, D. Wei, NO_2 sensing properties of WO_3 porous films with honeycomb structure, J. Alloy. Compd., 789 (2019) 129-138.

[10] Z. Li, A.A. Haidry, T. Wang, Z.J. Yao, Low-cost fabrication of highly sensitive room temperature hydrogen sensor based on ordered mesoporous Co-doped TiO_2 structure, Appl. Phys. Lett. 111 (2017) 032104.

[11] S. Capone, M. Benkovicova, A. Forleo, M. Jergel, M.G. Manera, P. Siffalovic, A. Taurino, E. Majkova, P. Siciliano, I. Vavra, S. Luby, R. Rella, Palladium/gamma-Fe_2O_3 nanoparticle mixtures for acetone and NO_2 gas sensors, Sens. Actuators B Chem. 243 (2017) 895-903.

[12] Z. Wu, Z. Li, H. Li, M. Sun, S. Han, C. Cai, W. Shen, Y. Fu, Ultrafast Response/Recovery and High Selectivity of the H_2S Gas Sensor Based on alpha-Fe_2O_3 Nano-Ellipsoids from One-Step Hydrothermal Synthesis, ACS Appl Mater Interfaces 11 (2019) 12761-12769.

[13] Z. Wu, Z. Li, H. Li, M. Sun, S. Han, C. Cai, W.g Shen,. Y.g Fu, Ultrafast Response/Recovery and High Selectivity of the H2S Gas Sensor Based on α□Fe_2O_3 Nano-Ellipsoids from One-Step Hydrothermal Synthesis, ACS Applied Materials & Interfaces, 11 (2019) 12761−12769.

[14] M.S. Choi, J.H. Bang, A. Mirzaei, W. Oum, H.G. Na, C. Jin, S.S. Kim, H.W. Kim,

Promotional effects of ZnO-branching and Au-functionalization on the surface of SnO_2 nanowires for NO_2 sensing, J. Alloy. Compd., 786 (2019) 27-39.

[15] X. Hu, Z. Zhu, C. Chen, T. Wen, X. Zhao, L. Xie, Highly sensitive H_2S gas sensors based on Pd-doped CuO nanoflowers with low operating temperature, Sens. Actuators B Chem. 253 (2017) 809-817.

[16] J. Wang, Z. Li, S. Zhang, S. Yan, B. Cao, Z. Wang, Y. Fu, Enhanced NH_3 gas-sensing performance of silica modified CeO_2 nanostructure based sensors, Sens. Actuators B Chem. 255 (2018) 862-870.

[17] Y. Wang, G. Duan, Y. Zhu, H. Zhang, Z. Xu, Z. Dai, W. Cai, Room temperature H_2S gas sensing properties of In_2O_3 micro/nanostructured porous thin film and hydrolyzation-induced enhanced sensing mechanism, Sens. Actuators B Chem. 228 (2016) 74-84.

[18] C.W. Na, J.H. Kim, H.J. Kim, H.S. Woo, A. Gupta, H.-K. Kim, J.H. Lee, Highly selective and sensitive detection of NO_2 using rGO-In_2O_3 structure on flexible substrate at low temperature, Sens. Actuators B Chem. 255 (2018) 1671-1679.

[19] A. Shanmugasundaram, V. Gundimeda, T. Hou, D.W. Lee, Realizing Synergy between In_2O_3 Nanocubes and Nitrogen-Doped Reduced Graphene Oxide: An Excellent Nanocomposite for the Selective and Sensitive Detection of CO at Ambient Temperatures, ACS Appl. Mater. Interfaces 9 (2017) 31728-31740.

[20] J. Hu, Y. Sun, Y. Xue, M. Zhang, P. Li, K. Lian, S. Zhuiykov, W. Zhang, Y. Chen, Highly sensitive and ultra-fast gas sensor based on CeO_2-loaded In_2O_3 hollow spheres for ppb-level hydrogen detection, Sens. Actuators B Chem. 257 (2018)

124-135.

[21] K.K. Kim, D. Kim, S.H. Kang, S. Park, Detection of ethanol gas using In_2O_3 nanoparticle-decorated ZnS nanowires, Sens. Actuators B Chem. 248 (2017) 43-49.

[22] S.S. Kim, J.Y. Park, S.W. Choi, H.G. Na, J.C. Yang, H.W. Kim, Enhanced NO_2 sensing characteristics of Pd-functionalized networked In_2O_3 nanowires, J. Alloy. Compd. 509 (2011) 9171-9177.

[23] B. Xiao, Q. Zhao, D. Wang, G. Ma, M. Zhang, Facile synthesis of nanoparticle packed In_2O_3 nanospheres for highly sensitive NO_2 sensing, New J. Chem. 41 (2017) 8530-8535.

[24] X. Liang, T.H. Kim, J.W. Yoon, C.H. Kwak, J.H. Lee, Ultrasensitive and ultraselective detection of H_2S using electrospun CuO-loaded In_2O_3 nanofiber sensors assisted by pulse heating, Sens. Actuators B Chem. 209 (2015) 934-942.

[25] L. Gao, Z. Cheng, Q. Xiang, Y. Zhang, J. Xu, Porous corundum-type In_2O_3 nanosheets: Synthesis and NO_2 sensing properties, Sens. Actuators B Chem. 208 (2015) 436-443.

[26] P.S. Khiabani, E. Marzbanrad, H. Hassani, B. Raissi, Fast Response NO_2 Gas Sensor Based on In_2O_3 Nanoparticles, J. Am. Ceram. Soc. 96 (2013) 2493-2498.

[27] K. Yao, D. Caruntu, Z. Zeng, J. Chen, C.J. O'Connor, W. Zhou, Parts per Billion-Level H_2S Detection at Room Temperature Based on Self-Assembled In_2O_3 Nanoparticles, J. Phys. Chem. C 113 (2009) 14812-14817.

[28] B. Shanmuga Priya, M. Shanthi, C. Manoharan, M. Bououdina, Hydrothermal

synthesis of Ga-doped In_2O_3 nanostructure and its structural, optical and photocatalytic properties, Mat. Sci. Semicon. Proc. 71 (2017) 357-365.

[29] H. von Wenckstern, D. Splith, F. Schmidt, M. Grundmann, O. Bierwagen, J. S. Speck, Schottky contacts to In_2O_3, APL Materials 2 (2014)046104.

[30] J. Michel, D. Splith, J. Rombach, A. Papadogianni, T. Berthold, S. Krischok, M. Grundmann, O. Bierwagen, H. Wenckstern, M. Himmerlich, Processing Strategies for High-Performance Schottky Contacts on n□Type Oxide Semiconductors: Insights from In_2O_3. ACS Appl. Mater. Interfaces 11(2019) 27073-27087

.

[31] J. Zhang, X. Liu, G. Neri, N. Pinna, Nanostructured Materials for Room-Temperature Gas Sensors, Adv. Mater. 28 (2016) 795-831.

[32] J. Hu, Y. Liang, Y. Sun, Z. Zhao, M. Zhang, P. Li, W. Zhang, Y. Chen, S. Zhuiykov, Highly sensitive NO_2 detection on ppb level by devices based on Pd-loaded In_2O_3 hierarchical microstructures, Sens. Actuators B Chem. 252 (2017) 116-126.

[33] Q. Yang, X. Cui, J. Liu, J. Zhao, Y. Wang, Y. Gao, P. Sun, J. Ma, G. Lu, A low temperature operating gas sensor with high response to NO_2 based on ordered mesoporous Ni-doped In_2O_3, New J. Chem. 40 (2016) 2376-2382.

[34] X. Li, S. Yao, J. Liu, P. Sun, Y. Sun, Y. Gao, G. Lu, Vitamin C-assisted synthesis and gas sensing properties of coaxial In_2O_3 nanorod bundles, Sens. Actuators B Chem. 220 (2015) 68-74.

[35] F. Gu, R. Nie, D. Han, Z. Wang, In_2O_3-graphene nanocomposite based gas sensor for selective detection of NO_2 at room temperature, Sens. Actuators B Chem. 219

(2015) 94-99.

[36] Z. Cheng, L. Song, X. Ren, Q. Zheng, J. Xu, Novel lotus root slice-like self-assembled In_2O_3 microspheres: Synthesis and NO_2-sensing properties, Sens. Actuators B Chem. 176 (2013) 258-263.

[37] W. Yang, P. Wan, X. Zhou, J. Hu, Y. Guan, L. Feng, Additive-Free Synthesis of In_2O_3 Cubes Embedded into Graphene Sheets and Their Enhanced NO_2 Sensing Performance at Room Ternperature, ACS Appl. Mater. Interfaces 6 (2014) 21093-21100.

[38] T. Siciliano, M. Di Giulio, M. Tepore, A. Genga, G. Micocci, A. Tepore, In_2O_3 films prepared by thermal oxidation of amorphous InSe thin films, Thin Solid Films 520 (2012) 2455-2460.

[39] S. Roso, C. Bittencourt, P. Umek, O. Gonzalez, F. Guell, A. Urakawa, E. Llobet, Synthesis of single crystalline In_2O_3 octahedra for the selective detection of NO_2 and H_2 at trace levels, J. Mater. Chem. C 4 (2016) 9418-9427.

[40] C. Zhao, B. Huang, E. Xie, J. Zhou, Z. Zhang, Improving gas-sensing properties of electrospun In_2O_3 nanotubes by Mg acceptor doping, Sens. Actuators B Chem. 207 (2015) 313-320.

[41] J. Liu, W. Guo, F. Qu, C. Feng, C. Li, L. Zhu, J. Zhou, S. Ruan, W. Chen, V-doped In_2O_3 nanofibers for H_2S detection at low temperature, Ceram. Int. 40 (2014) 6685-6689.

[42] W. Chen, Y. Liu, Z. Qin, Y. Wu, S. Li, P. Ai, A Single Eu-Doped In_2O_3 Nanobelt Device for Selective H_2S Detection, Sensors 15 (2015) 29950-29957.

[43] L. Yin, D. Chen, M. Hu, H. Shi, D. Yang, B. Fan, G. Shao, R. Zhang, G. Shao, Microwave-assisted growth of In_2O_3 nanoparticles on WO_3 nanoplates to improve H_2S-sensing performance, J. Mater. Chem. A 2 (2014) 18867-18874.

[44] M. Kaur, N. Jain, K. Sharma, S. Bhattacharya, M. Roy, A.K. Tyagi, S.K. Gupta, J.V. Yakhmi, Room-temperature H_2S gas sensing at ppb level by single crystal In_2O_3 whiskers, Sensors and Actuators B: Chemical 133 (2008) 456-461.

[45] A. Singhal, M. Kaur, K.A. Dubey, Y.K. Bhardwaj, D. Jain, C.G.S. Pillai, A.K. Tyagi, Polyvinyl alcohol- In_2O_3 nanocomposite films: synthesis, characterization and gas sensing properties, RSC Adv. 2 (2012) 7180-7189.

[46] J. Zhou, M. Ikram, A.U. Rehman, J. Wang, Y. Zhao, K. Kan, W. Zhang, F. Raziq, L. Li, K. Shi, Highly selective detection of NH_3 and H_2S using the pristine CuO and mesoporous In_2O_3@CuO multijunctions nanofibers at room temperature, Sens. Actuators B Chem. 255 (2018) 1819-1830.

[47] H. Duan, L. Yan, Y. He, H. Li, L. Liu, Y. Cheng, L. Du, The fabrication of In_2O_3 toruloid nanotubes and their room temperature gas sensing properties for H_2S, Mater. Res. Express. 4 (2017).

[48] Y. Huang, W. Chen, S. Zhang, Z. Kuang, D. Ao, N.R. Alkurd, W. Zhou, W. Liu, W. Shen, Z. Li, A high performance hydrogen sulfide gas sensor based on porous alpha-Fe_2O_3 operates at room-temperature, Appl. Surf. Sci. 351 (2015) 1025-1033.

[49] T. Wang, J. Hao, S. Zheng, Q. Sun, D. Zhang, Y. Wang, Highly sensitive and rapidly responding room-temperature NO_2 gas sensors based on WO_3 nanorods/sulfonated graphene nanocomposites, Nano Res. 11 (2018) 791-803.

[50] S.S. Shendage, V.L. Patil, S.A. Vanalakar, S.P. Patil, N.S. Harale, J.L. Bhosale, J.H. Kim, P.S. Patil, Sensitive and selective NO_2 gas sensor based on WO_3 nanoplates, Sens. Actuators B Chem. 240 (2017) 426-433.

[51] S. An, S. Park, H. Ko, C. Lee, Enhanced NO_2 gas sensing properties of WO_3 nanorods encapsulated with ZnO, Appl. Phys. A-mater. 108 (2012) 53-58.

[52] X. Liu, B. Du, Y. Sun, M. Yu, Y. Yin, W. Tang, C. Chen, L. Sun, B. Yang, W. Cao, M.N.R. Ashfold, Sensitive Room Temperature Photoluminescence-Based Sensing of H_2S with Novel CuO-ZnO Nanorods, ACS Appl. Mater. Interfaces 8 (2016) 16379-16385.

[53] Z. Li, H. Li, Z. Wu, M. Wang, J. Luo, H. Torun, P. Hu, C. Yang, M. Grundmann, X. Liu, Y. Fu, Advances in designs and mechanisms of semiconducting metal oxide nanostructures for high-precision gas sensors operated at room temperature, Mater. Horiz., 6 (2019) 470-506.

[54] L. Xu, B. Dong, Y. Wang, X. Bai, Q. Liu, H. Song, Electrospinning preparation and room temperature gas sensing properties of porous In_2O_3 nanotubes and nanowires, Sens. Actuators B 147 (2010) 531-538.